Available online at www.sciencedirect.com

jmr&t Journal of Materials Research and Technology

journal homepage: www.elsevier.com/locate/jmrt

Original Article

Investigation of expansion percentages and groove inclusions on the performance of welded, expanded, welded-expanded tube-to-tubesheet joints

Dinu Thomas Thekkuden [a], *Abdel-Hamid Ismail Mourad* [a,b,c,*], *Abdel-Hakim Bouzid* [d], *Muhammad M. Sherif* [e]

[a] *Mechanical and Aerospace Engineering Department, College of Engineering, United Arab Emirates University, Al-Ain, P.O. Box. 15551, United Arab Emirates*

[b] *National Water and Energy Center, United Arab Emirates University, Al Ain 15551, United Arab Emirates*

[c] *On Leave from Mechanical Design Department, Faculty of Engineering, El Mataria, Helwan University, Cairo, Egypt*

[d] *Ecole de Technologie Superieure, 1100 Notre-Dame Quest, Montreal, Quebec, H3C 1K3, Canada*

[e] *Civil, Construction and Environmental Engineering Department, School of Engineering, University of Alabama at Birmingham, Birmingham, USA*

ARTICLE INFO

Article history:
Received 13 October 2022
Accepted 7 December 2022
Available online 15 December 2022

Keywords:
Carbon steel
Heat exchanger
Roller expansion
Tube
Tubesheet
Tungsten inert gas welding

ABSTRACT

Tube-to-tubesheet joints play a crucial role in providing structural integrity to the shell and tube heat exchangers. This research investigated the combined effect of roller expansion percentages and grooves on the performance of expanded and welded-expanded tube-to-tubesheet joints. The results indicated that the joint strength of welded-expanded (except for 6% tube expansion and 2 grooves) and welded joints exceeded the nominal axial strength of the tube, 404.90 MPa. The highest tube pull-out strength of 290.77 MPa in the expanded only joint (10% tube expansion and 2 grooves), lesser than the axial strength of the tube by 28.25%, suggested avoiding the expansion process alone for 23 mm thick tubesheets. High dilution and inadequate minimum leak path (<1.78 mm) result in the failure of the welded-expanded joint. The highest hardness of 216 HV is formed at the weld zone comprising of α ferrite and widmanstatten ferrite. From 4% to 10% tube expansion percentages, the grains at the inner tube edges were refined from 8.33 μm to 6.25 μm at the expanded zone and from 9.09 μm to 6.66 μm at the transition zone due to intensive plastic deformation caused by the rollers. Grain refinement by expansion process resulted in high hardness of 182.3 HV and 156.1 HV at the inner tube edges of the expanded and transition zone, respectively. The grains were coarser, and hardness was less at the outer tube edges of expanded and transition zone. This study is promising for selecting the appropriate manufacturing process and conditions for the optimum performance of tube-to-tubesheet joints.

* Corresponding author.
E-mail address: ahmourad@uaeu.ac.ae (A.-H.I. Mourad).

https://doi.org/10.1016/j.jmrt.2022.12.045

1. Introduction

The strength of tube-to-tubesheet joints is vital for providing structural integrity to the shell and tube heat exchangers [1]. The quality of tube-to-tubesheet joints based on their mechanical and metallurgical properties depends on the manufacturing processes, process parameters and design configurations. The welding and tube expansion process are commercialized techniques for producing tube-to-tubesheet joints. Tungsten inert gas (TIG) welding is the most commonly used welding operation whereas either the roller expansion or hydraulic expansion processes are most prominent for the tube expansion process. In the case of TIG welding, the deposited weld electrode joins the tube and tubesheet forming a weld fusion zone. This weldment or weld bead acts as a sealant separating the tube-side and shell-side transfer fluids in shell and tube heat exchangers (See Fig. 1). In addition, tungsten inert gas welded coupons generally exhibit high strength with the optimum welding parameters [2]. Therefore, the exhibition of high joint strength and leak tightness are the major advantages of tube-to-tubesheet welds. On the other side, the residual stresses due to welding and weld brittleness have been reported previously as the main causes of the failure of the heat exchanger [3,4]. A high weld hardness as a result of inappropriate weld electrode and welding parameters also causes weld rupture [5]. Retubing for replacing the damaged welded tubes from the tubesheet is mandatory and rigorous [6]. This indicates that there are pros and cons to the welding of tube-to-tubesheet joints. In the case of tube expansion, the roller or hydraulic expansion exerts pressure on the inner tube surface radially outwards and this causes wall thinning of the tubes once the tubes come in contact with the tubesheet. As illustrated in Fig. 2, the wall thinning of tubes causes a reduction in the tube thickness. Therefore, the extent of tube wall thinning is expressed as tube wall reduction percentage or expansion percentage. As a result of tube expansion and subsequent contact of the tube with the tubesheet, the developed contact pressure between the tube and tubesheet provides strength to the tube-to-tubesheet joint. The residual contact pressure at the tube-to-tubesheet interface is directly proportional to the expansion percentage and tube pull-out strength [7]. The required expansion percentages vary depending on the tube and tubesheet materials. The range of expansion percentages recommended for the carbon steel is 5%–8% [8]. The tubes undergo intensive plastic deformation during the tube expansion process [9]. The major demerit of the tube expansion process is the absence of leak proof joint. Each of the manufacturing processes for tube-to-tubesheet joint has merits and demerits. Heat exchanger industries give wide attention for avoiding tube-to-tubesheet defects and on the other side, plant shutdowns are immediately called for the maintenance operation in case of any leakage encountered [10]. Furthermore, the manufacturing processes exhibit an unique impact to the mechanical and metallurgical characteristics of the joint. Therefore, the right selection of the manufacturing process requires a good understanding of the process, process parameters and their effects on the mechanical and metallurgical properties of tube-to-tubesheet joints.

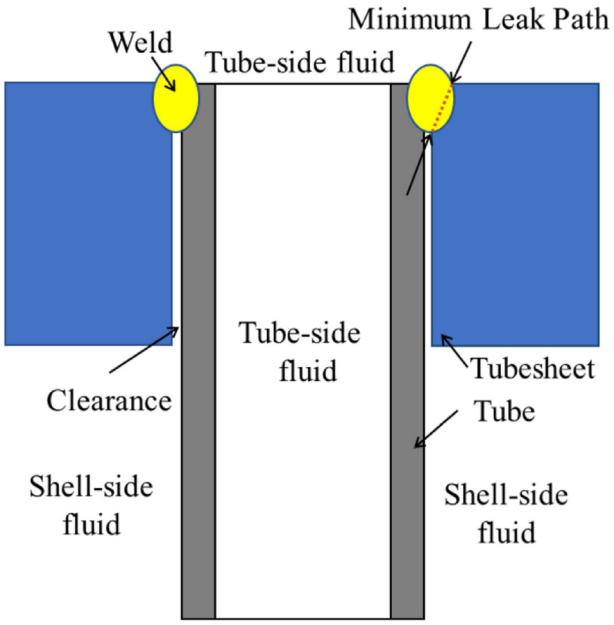

Fig. 1 – Tube-to-tubesheet weld separating the tube-side and shell-side fluids in shell and tube heat exchanger.

The welding parameters and expansion percentages are found to influence the tube pull-out strength of tube-to-tubesheet joints. Apart from the above factors, the design engineers consider the inclusion of grooves on the inner tubesheet holes for enhancing the pull-out strength. However, the number of grooves is uncertain for the optimum tube pull-out strength. In the hydraulic expansion process, the strength of the joints was found to increase with both the number of grooves and expansion pressure, but it was concluded only from simulation [11]. Ma et al. confirmed experimentally that both pull-out force and push-out force increase with the hydraulic expansion pressures, however after a certain expansion pressure, the strength decreases

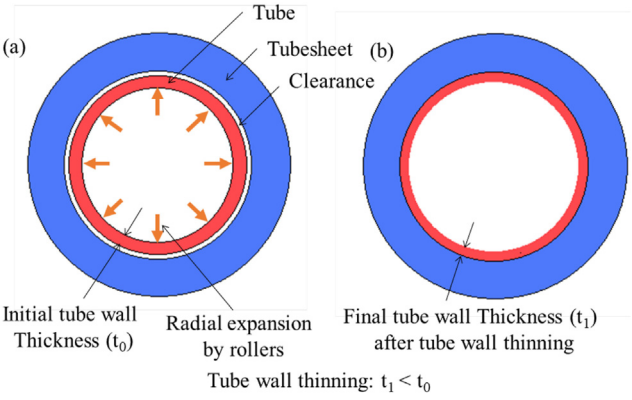

Fig. 2 – Tube expansion process: (a) Before expansion, (b) After expansion showing the wall tube thinning.

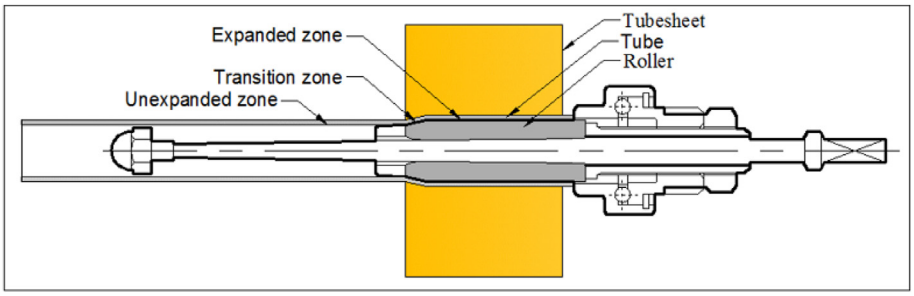

Fig. 3 – Schematic diagram showing the expanded zone, transition zone and unexpanded zone in the expanded tube using roller expansion process.

due to over-expansion [12]. An experimental study by Wang and Sang has illustrated that the groove width is the significant factor affecting joint strength over groove spacing and location [13]. The work of Qian et al. also ascertained that the pull-out force increases with the increase in the groove width [14]. According to Yoganathan et al., evenly thick tubes throughout the circumference are required for optimal tube pull-out strength, however, any thickness offset causes strength loss [15]. In another case, the protruded welded joints exhibit higher pull-out force and fatigue strength compared to flush joint and flush joints with U groove and 45° V groove [16]. Increased friction between the tube and tubesheet enhances the strength of the tube and tubesheet joints [17]. The joint strength and leak tightness of the tube and tubesheet joints are ensured by the sufficient contact pressure between the tube and tubesheet [18]. The Bauschinger effect, according to Bouzid et al. has a considerable impact on the lowering of residual contact pressure [19]. Also, the residual contact pressure decreases with the expansion of the neighbour adjacent tubes in the tubesheet [20]. The ligament efficiency and expansion sequence order, in addition to neighbour tube expansion, have a substantial impact on residual contact pressure [20]. The tube pull-out strength at the tube-to-tubesheet interface increases with the increase in the residual contact pressure. Literature indicates that the possible ways of enhancing the tube-to-tubesheet joint strength using the design configurations, material properties, process and process parameters are highly demanded topics of interest. It is worth noting that most of the above-mentioned findings were concluded only from numerical and analytical investigations. The experimental investigation of tube-to-tubesheet joints is less compared to the numerical and analytical studies. The experimentation in this research area is less because the expense incurred is huge and there are requirements for expensive manufacturing tools and expert operators. Moreover, most of the studies are restricted to the hydraulic expansion process and therefore, experimental studies on the roller expansion process are highly demanded.

Uniform pressure is exerted in the hydraulic expansion process, whereas localized pressure is applied by the rollers in the rolling expansion process. The expansion process by either hydraulic or roller expansion divides the tube zone into expanded zone, an unexpanded zone and, a transition zone between the expanded and unexpanded zone as shown in Fig. 3. The expanded zone in the tube is formed as a result of rigorous pressure being exerted on the inner tube surface [21]. The transition zone, close to the expanded zone, has exhibited high residual stresses [22,23]. The residual stress at the transition zone has been identified as one of the main reasons for the crack initiation at this zone in industrial-operated heat exchangers [24–26]. The intense plastic deformation in the expanded zone and the effect extended to the transition zone demands metallurgical investigation. However, the metallurgical investigation especially on the expanded zone and transition zone is lacking in the literature.

Based on the research gaps mentioned at the end of the above paragraphs, the main objective of the current work is to investigate the mechanical and metallurgical properties of tube-to-tubesheet heat exchanger joints produced using three kinds of fabrication methods such as expansion, welding and hybrid welding-expansion. The combined effect of tube expansion percentages and number of grooves on the mechanical and metallurgical properties of tube-to-tubesheet joints, lacking in the literatures, is investigated from the expanded and hybrid welded-expanded joints. Finally, the influence of the expansion percentages on the mechanical and metallurgical properties at the expanded zone and transition zone of tubes are evaluated. This research is expected to be very promising for researchers and professionals working in the area of metallurgy, joining, materials and heat exchangers.

Table 1 – Chemical composition of ASTM A179 Tube from optical emission spectroscopy.

Element	C	Mn	Si	S	P	Cr	Ni	Cu	Ti	Al
%	0.112	0.473	0.217	0.0029	0.0089	0.0664	0.0213	0.0206	0.0022	0.0240
Element	N	Mo	V	Nb	W	Pb	Sn	As	Zr	Bi
%	0.0094	0.0046	<0.0005	0.0025	0.0071	0.0166	0.0042	0.0036	<0.0010	0.0069
Element	Ca	Sb	Se	Te	Ta	N	Zn	Co	Fe	CEV
%	0.0015	0.0396	0.0042	0.0182	<0.007	0.0094	<0.001	<0.001	98.9	0.208

Table 2 – Chemical composition of SA 516 Gr.70 tubesheet.

Element	C	Mn	Si	S	P	Cr	Ni	Cu
%	0.18	1.185	0.22	0.012	0.018	0.025	0.02	0.02
Element	Ti	Al	N	Mo	V	Nb	Fe	CEV
%	0.0135	0.025	0.005	0.003	0.003	0.0315	97.847	0.385

2. Materials and methods

ASTM A179 tube and SA 516 Gr. 70 tubesheet, widely used for many heat exchanger applications, were chosen as parent materials. Table 1 and Table 2 provided the chemical compositions of ASTM A179 and SA 516 Gr. 70 materials, respectively. ASTM A179 seamless tubes were having 19.1 mm outer diameter and 2.67 mm tube wall thickness. Individual square tubesheet mock-up blocks with 50 mm × 50 mm X 23 mm dimensions with a drilled tube hole of 19.30 mm diameter at the centre were manufactured. Based on the outer diameter of the tube and diameter of hole cut in the tubesheet, the radial clearance was 0.1 mm. Tubesheets with one groove, two grooves and without any grooves on the inner surface of tubesheet hole were prepared for investigating the effect of grooves on the pull-out strength at various expansion percentages (See Fig. 4). The groove width and groove depth were 3 mm and 1 mm, respectively. The manufacturing processes of tube-to-tubesheet such as expansion, welding and hybrid welded-expansion were performed. The tungsten inert gas welding was performed using JASIC TIG 200 Pulse AC/DC Mini Inverter Welder powersource and ER AWS A5.18: ER70S-6 (Bohler S EMK 6) filler rod. Chemical composition of ER70S-6 is provided in Table 3. The welding was performed with a single weld pass at ambient atmospheric temperature. The welding parameters were set to 2.40 mm diameter consumable rod, direct current electrode negative (DCEN) configuration, uphill progression and pure Argon shielding gas with a flow rate of 30 cfh. The rolling expansion process was performed using Elliott expansion equipment comprising of an electronic expansion control unit, expander and three rollers. The tubes were expanded using tube wall reduction percentages or expansion percentages of 4%, 6%, 8% and 10% in single grooved, double grooved and without grooved tube-to-tubesheet joints. The initial inner diameter of the tube, 13.76 mm, was expanded to 14.07 mm, 14.19 mm, 14.28 mm and 14.37 mm using 4%, 6%, 8% and 10% expansion percentages respectively. In the case of expanded joints, the tubes are expanded throughout the tubesheet thickness. The expansion length or roller length in expanded joints was 23 mm. For the hybrid welded and expanded joints, the welding was performed first which was followed by expansion. For the case of expansion after welding, the expansion over the entire tubesheet thickness is inappropriate as it would cause damage to the weld. Therefore, rolling expansion was performed with an expansion length of 15 mm and 3 mm away from the weld in hybrid welded-expanded joints. The liquid penetration test, macro examination, micro examination, minimum leak path, pull-out test and hardness test were conducted for the qualification of tube-to-tubesheet joints. The tube pull-out test was performed using a universal testing machine with a capacity of 1000 kN as shown in Fig. 5 in accordance with ASME SEC. VIII DIV. I ED. 2019 - Appendix A. The tube end opposite to the tube-to-tubesheet joint is plugged with a cylindrical rod for preventing tube deformation or tube rupture while gripping in the upper jaw of the universal testing machine. The toughness of the tube subjected to tube pull-out load and those fractured at the tube were estimated using the area under the stress-strain curve. The macro examination was performed in accordance with the standard ASME SEC IX Ed. 2019. The minimum leak path was measured from the macroscopic image at 10X. The quality assessment of tube-to-tubesheet weld joints based on minimum leak path was evaluated using ASME SEC. IX Ed. 2019-QW-193.1.3 standard. Vickers hardness was measured at the base material, weld zone, and heat affected zones on the tube side and tubesheet side with a test load of 10 kgf using Wilson UH250 Universal Hardness Tester. The qualification of the hardness was verified using NACE MR0175. The hardness at the expanded and transition zones was tested by applying 1 kgf load. The samples were grinded using 120, 180, and 240 grid waterproof silicon carbide paper, then cloth polished for optical macroscopic examinations. For optical microscopy using Panthera TEC MAT, the samples were ground with P120, P240, P320, P600, P1000, and P1200 grid silicon carbide sheets, then cloth polished with 6 μm and 3 μm diamond particles for optical microscopic examination. After washing with pure ethanol, the polished mirror-like samples were etched for 45 s with 2.5% Nital (97.5 ml ethanol + 2.5 nitric acid). The grain size is determined using Heyn intercept method. A SHIMADZU Lab X-XRD-6100 X-ray diffractometer with a Cu–K X-ray line (=1.5418) operating at 40 kV with a current of 30 mA was used to analyze X-ray diffraction (XRD) of the weld metal for phase identification. With a 0.02°/min step size, the spectra were captured from 20° to 100°. For phase identification, the XRD profiles were compared to the PDF-2 database.

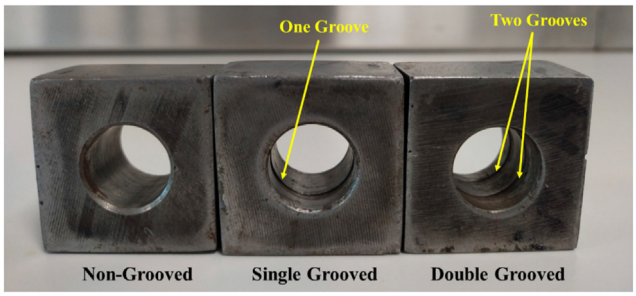

Fig. 4 – Tubesheet blocks with and without grooves.

Table 3 – Chemical composition of ER 70S-6 filler rod from the specification sheet.

Element	C	Mn	Si	P	S
%	0.07	1.48	0.85	0.02	0.015

Fig. 5 – Tube pull-out test setup using universal testing machine.

3. Results and discussion

3.1. *Liquid penetration test*

The liquid penetration test is the preliminary non-destructive quality inspection technique for assessing the quality of the tube-to-tubesheet welds [27,28]. The quality of weldments in hybrid welded-expanded tube-to-tubesheet joints was examined with a liquid penetration test in accordance with ASME Sec V, Article 6. Fig. 6 shows the hybrid welded-expanded specimens inspected using liquid penetrant test. The results show that the welded specimens were free from any of the linear and rounded red indications. In the presence of surface flaws, the penetrant entering into the fissures is absorbed by the coated developer, forming the visible red indicator once the developer sets. The absence of visible red indication proved that the welds were free of surface defects. The quality of welded tube-to-tubesheet joints is assured as superior before evaluating the mechanical and metallurgical investigations of tube-to-tubesheet joints.

3.2. *Tube pull-out load*

The strength of welded, expanded and welded-expanded tube-to-tubesheet joints are evaluated from the load versus displacement using tube pull-out tests. The tube pull-out loads of tube-to-tubesheet joints are inspected based on ASME Sec VIII, DIV-1 for the qualification of the joints. According to the ASME Sec VIII, DIV-1, the tube and tubesheet joints are qualified if the joint strength is greater than the axial strength of the tubes [29]. The tube and tubesheet joints, on the other hand, are disqualified if the fracture occurs at the joint or the tube slips out from the tubesheet under the action of tensile force during the tube pull-out test.

3.2.1. *Hybrid welded-expanded tube-to-tubesheet joints*

The specimens of the hybrid welded-expanded tube and tubesheet joints subjected to tube pull-out tests are shown in Fig. 7. Fig. 8 shows the three fractured tubes of welded tube-to-tubesheet joints. After the tube pull-out test, all the hybrid welded-expanded tube and tubesheet samples were fractured

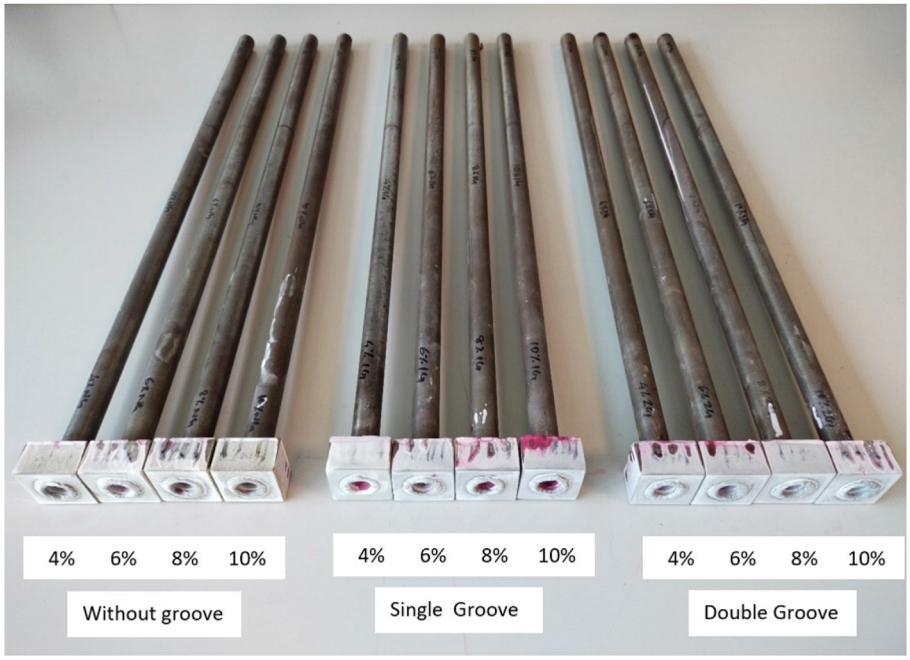

Fig. 6 – Liquid penetrant testing of hybrid welded-expanded tube-to-tubesheet joints.

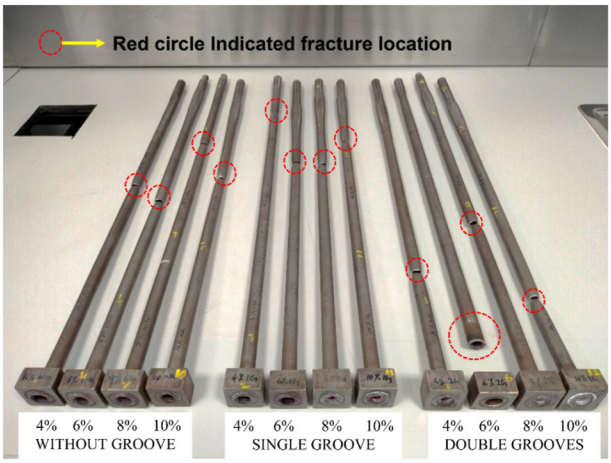

Fig. 7 – Fractured hybrid welded-expanded tube and tubesheet joints after tube pull-out test.

at the tubes, with the exception for the combination of 6% tube wall reduction and two grooved (2G) tubesheet where the failure was at the weld joint. Fig. 9 illustrates the pull-out load of tube-to-tubesheet joints for welded, expanded and hybrid welded-expanded conditions. The tube pull-out force of tube fractured hybrid welded-expanded samples was constant with an average of 56.50 kN. The axial tube strength corresponding to the 56.50 kN is 409.98 MPa. The fracture at the tubes in tube pull-out tests demonstrated that the strength of tube-to-tubesheet joints for specimens ruptured at the tube was certainly greater than 409.98 MPa. i.e., the strength of tube and tubesheet joints clearly exceeded the axial strength of the tubes. These welded-expanded joints having pull-out strength greater than the axial tube strength are qualified, according to ASME Sec-VIII, DIV-1, Non-Mandatory Appendix A, Basis for Establishing Allowable Loads for Tube To-Tube-Sheet Joints [30]. On the contrary, there is a slight depreciation of the tube pull-out force in hybrid welded and 6% expanded for 2 grooved configuration joint resulting in only 53.52 kN tube pull-out

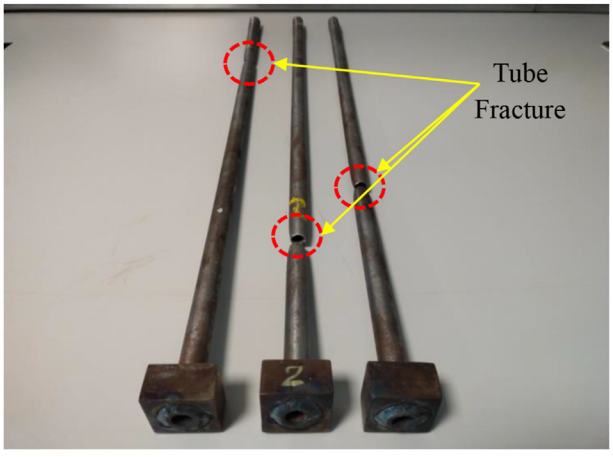

Fig. 8 – Fractured welded tube and tubesheet joints after tube pull-out test.

force. The corresponding joint failed at the tube-to-tubesheet weld joint without causing any fracture to the tubes. As a result, this tube and tubesheet joint is disqualified because the strength of the tube-to-tubesheet joint for the hybrid welding and 6% expansion case is less than the axial tube strength. The defective welds and inappropriate weld parameters are known to significantly degrade the strength of the joints [31,32]. Partial penetration tube-to-tubesheet welds as a result of inadequate arc heat input and bad welding parameters are found to reduce the load-bearing capacity of joints considerably [33]. The reasons for the failure of hybrid welded-6% expanded two grooved joint are anticipated due to the inappropriate weld bead characteristics, lack of weld penetration to the tube and tubesheet materials, low expansion percentage and lack of adequate contact pressures or expansion percentage. For the cases where tubes were fractured, toughness was measured using the area under the stress-strain curve considering the original cross-sectional area and elongation of the tube [34,35]. The qualified tube-to-tubesheet joints exhibited high capability to absorb the energy during the tube pull-out test. The material toughness of the tubes that were subjected to tensile load during tube pull-out test were 77.40 kJ/m^3 (4% NG), 86.13 kJ/m^3 (4% 1G), 76.30 kJ/m^3 (4% 2G), 84.49 kJ/m^3 (6% NG), 77.13 kJ/m^3 (6% 1G), 87.26 kJ/m^3 (8% NG), 79.00 kJ/m^3 (8% 1G), 84.49 kJ/m^3 (8% 2G), 77.69 kJ/m^3 (10% NG), 75.07 kJ/m^3 (10% 1G) and 76.83 kJ/m^3 (10% 2G). In all the cases of expanded joints and welded-expanded joint (6% tube expansion and 2 grooves) where failure occurred at the joints, the stress-strain were unable to plot for measuring the toughness due to uncertainty in the cross-sectional area and elongation.

3.2.2. *Expanded tube-to-tubesheet joints*

In the absence of welding and for the case of the expanded tube and tubesheet joints with expansion percentages ranging from 6% to 10%, the tube pull-out force increased with the presence of grooves at specific expansion percentages. From 6% to 10% expansion percentages, the maximum load bearing capacity increased from 8.3 kN to 14.8 kN for non-grooved condition, 9.25 kN–25.2 kN for one grooved condition and 12.35 kN–39.95 kN for two grooved condition. Therefore, the presence of grooves of up to two is found efficient in increasing the tube pull-out force by allowing the tube to bulge inwards to the groove, providing an interlocking mechanism. It is worth to note that the higher the expansion percentages, the greater the marginal difference in the tube pull-out force and the higher the effect of grooves. However, the tube pull-out force decreased in the presence and increasing the number of grooves for 4% expanded tube-to-tubesheet joints. Lack of sufficient expansion percentage for causing bulging of the tube is the major reason for the ineffectiveness of grooves [11]. Furthermore, the contact surface area between the tube and tubesheet is also a significant factor affecting the tube pull-out force. The theoretical pull-out force is directly proportional to the contact stress, outer tube radius, coefficient of friction and effective expansion length [36]. In the absence of tube bulging at low expansion percentages, the presence of grooves significantly reduced the contact surface area of the tube and tubesheet. In 4% expanded samples, the least pull-out force is obtained for two grooved joints (0.9 kN) and the highest for the

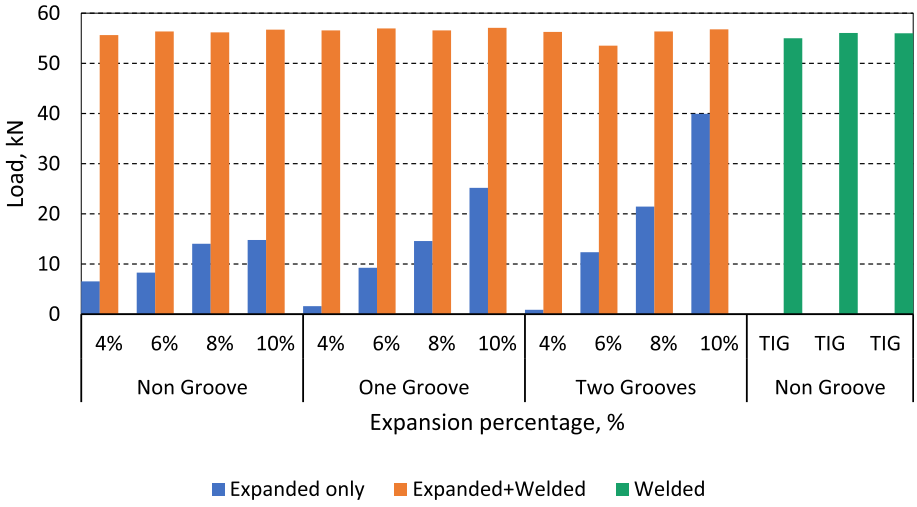

Fig. 9 – Tube pull-out force of welded, expanded and welded-expanded specimens.

joint without grooves (6.55 kN). For a certain expansion percentage, the contact stress and presence of grooves are concluded to act as superior factors affecting the tube pull-out force.

When each of the tube-to-tubesheet with specific groove categories is considered, the pull-out force increased with the increase in the expansion percentages. All twelve tubes were pulled out from the tubesheet during the tube pull-out test and the tubes were not fractured. The maximum tube pull-out force is obtained for 10% expanded two grooved joint with a value of 39.95 kN. None of the joint loads has exceeded 56.5 kN load which corresponds to the maximum load-bearing capacity of the tubes. As a result, all the expanded tube and tubesheet joints were disqualified since the joint strength was less than the axial tube strength. The major factor that changes the pull-out force for a fixed expansion percentage, according to the theoretical pull-out force calculations, is effective expansion length. I.e., the strength of the joint increases with the rise in the effective expansion length and viceversa. Therefore, the effective expansion length and thickness of the tubesheet affect the tightness of tube-to-tubesheet joints and the effective expansion length depends on the thickness of the tubesheet [37]. In this study, the thickness of the tubesheet is 23 mm and the maximum roller expansion effective length is limited to 23 mm. Heavy expansion with a 10% expansion percentage has not resulted in tube pull-out strength exceeding the axial tube strength of 409.98 MPa. The study clearly indicated that a 23 mm thick carbon steel tubesheet was inappropriate for the heat exchanger tube-to-tubesheet joint depending solely on the tube expansion process. The findings strongly advise using thicker tubesheet and the use of longer expansion length to achieve high tube-to-tubesheet joint strength.

3.2.3. *Welded tube-to-tubesheet joints*

If the manufacturing process chosen is welding alone without being expanded, the grooves on the tube hole have no role in enhancing the strength and therefore, only three welded joints in non-grooved condition were inspected. The welded tube-to-tubesheet joints were fractured at the tubes away from the joint. Therefore, the welded joint also exhibited a high weld strength greater than the axial tube strength. The maximum load-bearing capacity of the weld joint has exceeded 55 kN, 56.06 kN and 56 kN for the three cases. It is worth to note that the maximum load bearing capacity or joint strength of these three welded joints and eleven hybrid welded-expanded joints were not possible to estimate due to the fracture at the tubes. Also, nearly the same strength close to 56 kN represented only the maximum load-bearing capacity of tubes. It was anticipated that there would have been considerable differences in the joint strength for all those specimens fractured at tubes but it was not possible to evaluate unless the fracture occur at the joint. However these joints, welded-expanded and welded, are qualified based on ASME VIII. Div 1 since the joint strength exceeded the axial tube strength. In terms of tube pull-out strength, the tube fracture of welded-expanded (except for 6% tube expansion and 2 grooves specimen) and welded joints indicated that welding without roller expansion was sufficient for the qualification of tube-to-tubesheet joints based on tube pull-out test. By using the sole welding process for the production of tube-to-tubesheet joints, the cost is estimated to reduce considerably by avoiding both the use of roller expansion process in hybrid joining technique and manufacturing operation for cutting grooves inside the tubesheet hole. Therefore, the optimum manufacturing process for producing tube-to-tubesheet joint with adequate strength for 23 mm thick tubesheet is to the use of sole tungsten inert gas welding process.

3.3. *Minimum leak path*

The minimum leak path is the least distance needed by the transfer fluid to leak from the weld root to the exposed opposite side. The weldment acts as a barrier between the tube-side and shell-side fluids. For this reason, the minimum leak path is measured from the macrostructures. The macrostructures of twelve tube-to-tubesheet weld sectioned joints at 10× magnification are shown in Fig. 10. The welds were

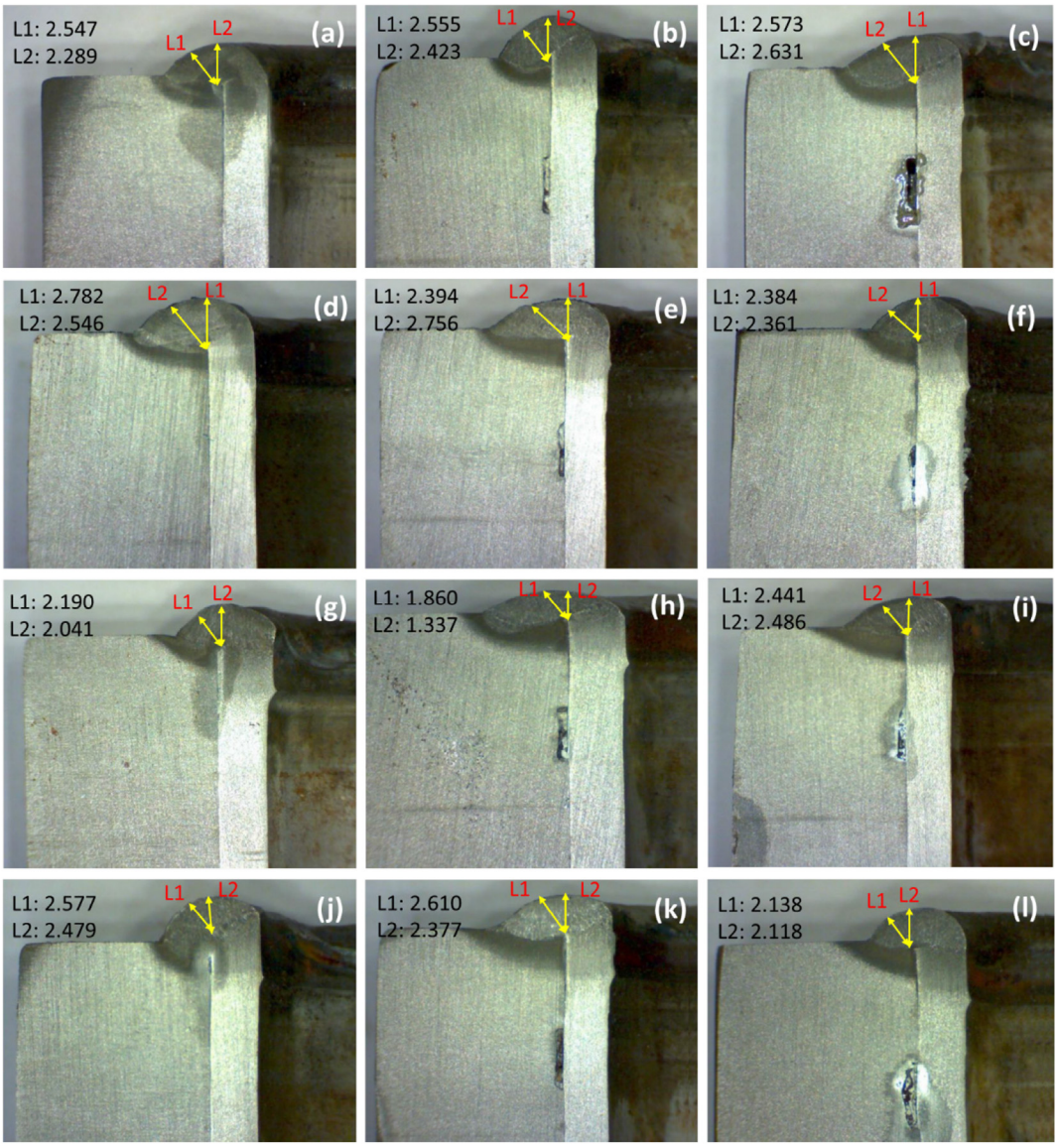

Fig. 10 – Minimum leak path of welded-expanded joints from the macroscopic image at 10X: (a) 4%-NG, (b) 4%-1G, (c) 4%-2G, (d) 6%-NG, (e) 6%-1G, (f) 6%-2G, (g) 8%-NG, (h) 8%-1G, (i) 8%-2G, (j) 10%-NG, (k) 10%-1G and (l) 10%-2G.

found free of porosities, blow holes and slag impurities. Furthermore, the weld materials were observed to have excellent penetration and sidewall fusion to the base materials. Two measurements of the leak path evaluated for each of the ten welds magnified at 10× are provided in Table 4. The least of the leak path, minimum leak path, is used for the qualification of welds in hybrid welded-expanded joints. Clause QW-193.1.3 (a) and (e) (Acceptance Criteria — Macro-Examination, Tube-to-tubesheet tests) in ASME SEC IX, 2004 edition is used for qualifying the tube-to-tubesheet joints [38]. The welds with minimum weld throat greater than two-thirds of tube thickness are considered qualified based on ASME SEC IX standard [39]. The tube thickness is 2.67 mm and two-thirds of the tube thickness is 1.78 mm. The minimum leak path for each of the twelve welds except for the case of welded followed by 8% tube expansion and 1 groove has exceeded 1.78 mm satisfying the qualification criteria. The welded-expanded specimen with 8% tube expansion and 1 groove condition is disqualified based on QW-193.1.3, ASME SEC IX due to minimum leak path of 1.33 less than the required 1.78 mm. The measurement of minimum leak path is a destructive technique where the specimens had to be sectioned and the sectioned surface had to be examined for the measurement of minimum leak path. Therefore, the minimum leak path measurements were not estimated for the specimens that were undergone tube pull-out tests. The bad welding, inappropriate weld bead characteristics and inadequate minimum leak path were concluded as the main reason for the failure of the joint for the tube pull-out specimen with conditions such as 6% tube expansion and 2 groove. In certain cases, the manufacturers set an optional non-standard stringent criterion for the qualification of minimum leak path where the minimum leak path should be greater than the tube thickness. The twelve tube-to-tubesheet

Table 4 – Minimum leak path measurements.

Tube wall reduction percentage	Groove condition	Dilution	Leak path		Minimum Leak Path, MLP	Qualification criteria	
			Length, L1	Length, L2	Minimum of L1 and L2	Tube thickness (Non-standard)	Two-thirds of tube thickness (Standard)
%	–	%	mm	mm	mm	mm	mm
4	NG	59.57	2.547	2.289	2.289	<2.67 (DQ)	>1.78 (Q)
4	1G	44.16	2.555	2.423	2.423	<2.67 (DQ)	>1.78 (Q)
4	2G	62.17	2.573	2.631	2.573	<2.67 (DQ)	>1.78 (Q)
6	NG	48.22	2.782	2.546	2.546	<2.67 (DQ)	>1.78 (Q)
6	1G	53.35	2.756	2.394	2.394	<2.67 (DQ)	>1.78 (Q)
6	2G	68.39	2.384	2.361	2.361	<2.67 (DQ)	>1.78 (Q)
8	NG	67.28	2.190	2.041	2.041	<2.67 (DQ)	>1.78 (Q)
8	1G	59.12	1.860	1.337	1.337	<2.67 (DQ)	<1.78 (DQ)
8	2G	57.84	2.441	2.486	2.441	<2.67 (DQ)	>1.78 (Q)
10	NG	54.55	2.577	2.479	2.479	<2.67 (DQ)	>1.78 (Q)
10	1G	56.41	2.610	2.377	2.377	<2.67 (DQ)	>1.78 (Q)
10	2G	67.08	2.138	2.118	2.118	<2.67 (DQ)	>1.78 (Q)

Note: 'Q' stands for qualified and 'DQ' stands for disqualified; NG: No groove; 1G: one groove; 2G: two grooves.

welds were considered as disqualified having the minimum leak path less than the tube wall thickness of 2.67 mm. However, this non-standard approach is rarely used as qualification criteria for qualifying the tube-to-tubesheet welds. The factors determining the minimum leak path, barrier between the tube and shell side fluids, are the weld penetration and dilution. The lesser the minimum leak path, the lesser is the weld penetration. High dilution causes an abrupt reduction in the corrosion resistance, hot-cracking resistance and mechanical properties such as strength and toughness [40]. The range of dilution in TIG welding lies between 10% and 70% [41]. The highest dilution in the welded-expanded joints was 68.39% and lowest dilution was 44.16%. Furthermore, the dilution of most of the welded-expanded joints higher than 50%, suggest that the quality of the welds is inappropriate. High dilution is formed by the melting of the tubes rather than the fusion of the filler material to the tubesheet. To prevent the high dilution in this case, it is recommended to use less heat input, thin welding electrodes and optimum weld passes. Therefore, the causes for the failure of hybrid welded and 6% expanded joint failure were concluded to be mainly due to the lack of weld penetration and high dilution.

3.4. *Weld metallurgy*

The microstructures at the different zones of welded tube and tubesheet joints at 200 X and 500 X are shown in Fig. 11. The base material of the ASTM A179 tube exhibited the presence of pearlite colonies across the polygonal ferrite. The pearlite bands and equiaxed ferrite constituted the microstructure of SA 516 Gr. 70 tubesheet. The peculiar behaviour of low-carbon steels is the excessive presence of the ferritic phase compared to the pearlite [42]. The elemental percentage of carbon from the optical emission spectroscopy lying below 0.3% further validated that the materials are of low-carbon steels. The tensile strength and hardness decrease with higher presence of ferrite in low carbon steels [43]. It was observed that the seamless A 179 tube has less strength and hardness due to the high presence of ferrite compared to SA 516 Gr. 70 tubesheet. The grain size of ASTM A179 tube base material was 14.2 μm (ASTM 9.5) whereas the grain size of SA 516 Gr. 70 tubesheet base material was 10.0 μm (ASTM 10). The grain size evaluation using Heyn intercept method lacks accuracy in general, however the measured grain sizes represent the near actual value. Due to the action of welding arc heat dissipation and subsequent cooling, heat affected zones are present at the adjacent region in tube and tubesheet joining to the weld zone. Fine grains are formed at the tube-side heat affected zone and tubesheet-side heat affected zones. These adjacent regions closer to the weld zone is subjected to heat dissipation. Zhao et al. stated that the temperature margin above the recrystallization temperature is narrower, limiting grain growth and enlargement in heat-affected zones [44]. Furthermore, shorter recrystallization time at the heat affected zones resulted in smaller grains compared to the adjacent base materials. Enlarged austenite grains usually form at the coarse-grained heat affected zones of heat treated plain carbon steels and low alloy steels that were subjected to isothermal heat treatments and forced cooling [45]. In this case, the slow cooling of tube-to-tubesheet welds exposed to environmental temperature and lack of isothermal heat treatments of the weld joints limited the formation of unusual enlarged sized austenite grains at the heat affected zones. In addition, lath martensite, forming as a result of high undercoolings in low carbon steels [46], were absent at the HAZ due to slow cooling of the tube-to-tubesheet weld joints. The weld zone is comprised of polygonal ferrite along with widmanstätten ferrite (WF). The widmanstatten ferrite is the saw tooth needle-shaped morphological form of ferrite emanating from the grain boundaries.

The Xray diffraction pattern analysis was conducted for analysing the ferrite phases at the ASTM A179 tube base material, SA 516 Gr. 70 tubesheet base material and weld zone (Fig. 12). The low carbon steel tube and tubesheet materials exhibited the presence of alpha ferrite whereas the austenite and delta ferrite were absent in these base materials. Similarly, the existence of ICDD 98-006-0826 coded α ferrite was confirmed at the weld zone by the three distinct peaks at

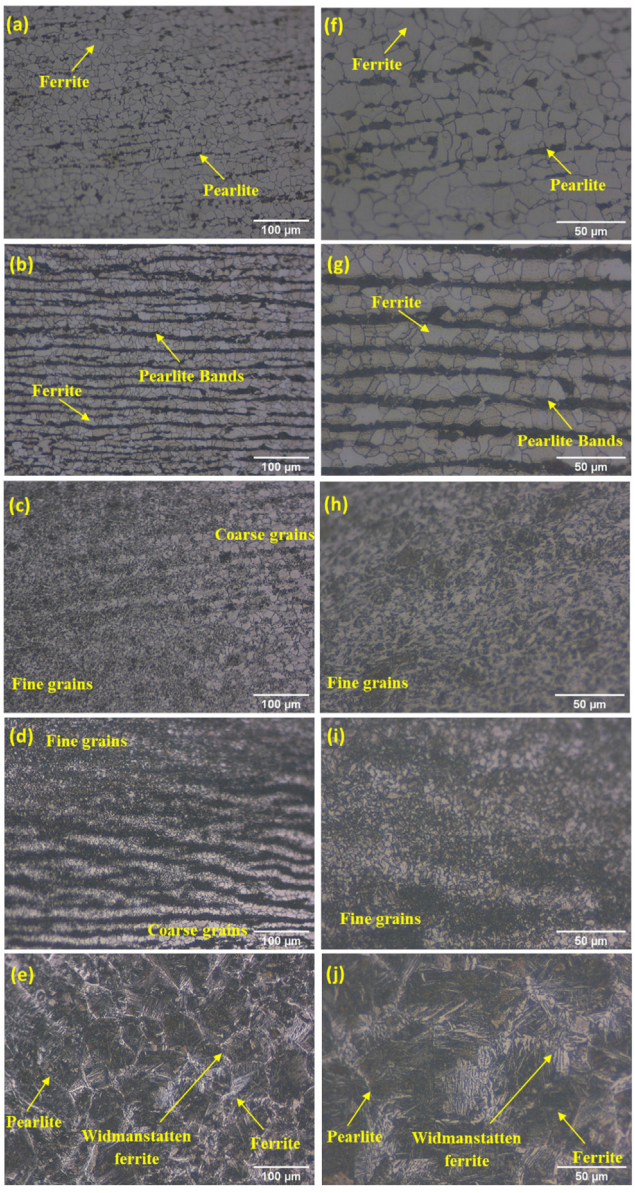

Fig. 11 – Optical microstructures: 200X (a) Base material-ASTM A179 M tube, (b) Base material-SA 516 Gr. 70 tubesheet, (c) HAZ at tube side, (d) HAZ at tubesheet side and (e) Weld zone; 500X (f) Base material-ASTM A179 M tube, (g) Base material-SA 516 Gr. 70 tubesheet, (h) HAZ at tube side, (i) HAZ at tubesheet side and (j) Weld zone.

$2\theta = 44.47°$ (Ref: 44.68°), $2\theta = 64.69°$ (Ref: 65.03°) and $2\theta = 82.06°$ (Ref: 82.34°). The delta and austenitic ferrite phases were absent at the weld zone in the XRD plot. The lower percentage of carbon in low carbon steel-based base materials and slow cooling process caused the absence of the austenitic ferrite phase at the weld zone [47].

3.5. *Weld hardness*

The hardness of the tube-to-tubesheet joints in heat exchangers must be within an acceptable limit. There are several consequences resulting in the failure of heat exchangers after exceeding the hardness beyond a particular level. For tube and tubesheet materials made of carbon steels, the acceptable limit according to NACE MR0175 is 250 HV. A high weld hardness was known to induce sulphide stress corrosion, stress-oriented hydrogen-induced cracking and soft zone cracking at the heat exchanger tube and tubesheet joints [4,48]. SA 516 Gr. 70 carbon steel, currently investigated in this study, was reported to have cracks after exposing 317 HV SA 516 Gr.70 weld to an H2S environment [49]. Fig. 13 illustrates the hardness of the tube, tubesheet, heat affected zones of tube and tubesheet and weld zone. According to NACE MR0175, the maximum hardness at the weld zone in the current study is 218 HV, which is less than the critical hardness limit of 250 HV for carbon steel welds joints. The highest hardness is observed at the weld zone with a mean value of 215.5 HV. Several additives in the weld electrode that are intended for enhancing the mechanical and metallurgical properties of the weld are the reason for the exhibition of high hardness at the weld zone. The alloying elements such as manganese, chromium and vanadium in electrodes tend to increase the hardness at the weld zone [50]. In terms of producing high hardness at the weld zone, carbon content has less of an impact than alloying components in low carbon steels. On the other side, it was also known that the morphological widmanstätten ferrite formed at the weld zone as a result of the cooling process after welding exhibited higher hardness than polygonal ferrite [51]. The tube and tubesheet base materials have an average hardness of 139.6 and 153.6 HV, respectively. SA 516 Gr.70 tubesheet has a higher carbon equivalent and pearlite content than A179 tubes, which contributes to its high hardness. The hardness in the heat affected zone was found to be greater than that of the corresponding tube and tubesheet base materials. The mean hardness at the tube heat affected zone and the tubesheet heat affected zone is 157.3 HV and 165 HV, respectively. Fine grains exhibit high hardness compared to coarsened base materials. Heat affected zones are fine grain sized. In heat-affected zones, the duration of temperature above the recrystallization temperature is limited, restricting grain coarsening [44].

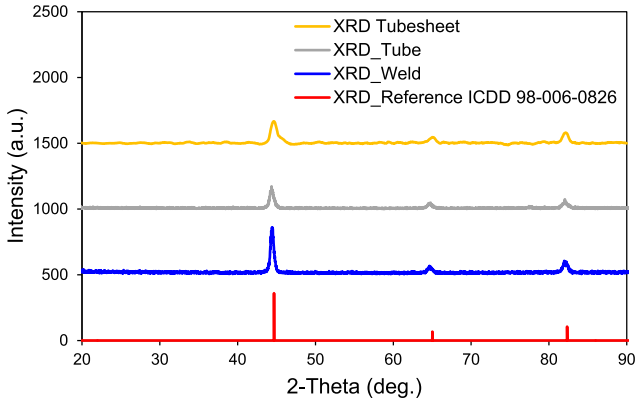

Fig. 12 – XRD analysis of Tube, tubesheet and tube-to-tubesheet weld zone.

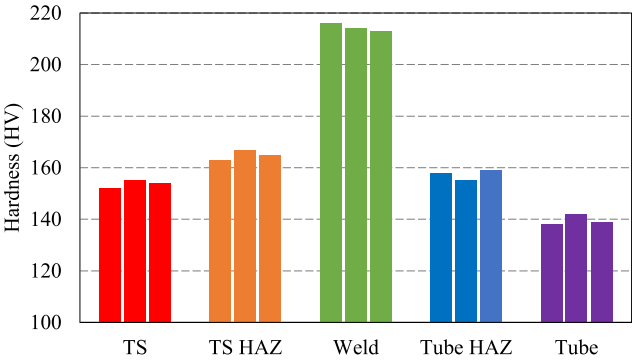

Fig. 13 – Vickers hardness at parent materials, heat affected zones and weld zone [TS: Tubesheet; HAZ: Heat affected zone].

3.6. *Tube expansion metallurgy and hardness*

The tubes are expanded by the roller expansion process at 4%, 6%,8% and 10% expansion percentages. In the expansion process, three zones are developed on the tube such as expansion zone, transition zone and unexpanded zone. The inner surface of the expanded tube was expanded by direct contact with the expander rollers while the outer surface of the expanded tube was contacted with the tubesheet during the expansion process. The transition zone with a slope was developed in the tube between the expanded zone and the unexpanded tube zone. Fig. 14 shows the microstructures of the outer and inner edges of the expanded tube zone. The grain sizes are evaluated using Heyn intercept method, however the measured grain sizes represent the close actual value. The grain sizes at the outer edge of the expanded tube zone for 4% and 6% are 10 μm and 9.09 μm respectively. The grain sizes were reduced to 7.69 μm by 8% and 10% tube expansion percentages. The tube strength at 4% expanded is only 6.55 kN for non-grooved condition. The lowest tube pull-out strength indicates that the tube has only come in slight contact with the tubesheet. At the lowest expansion percentages, contact pressure at the outer tube surface is inadequate. Therefore, the compressive stress on the outer tube by the tubesheet is less at lower expansion percentages. On the other side, the strength increased up to 14.8 kN using 10% expansion percentage. An adequate wall thinning, and high strength indicated the presence of considerable contact pressure. This intensive deformation at a 10% expansion percentage on the

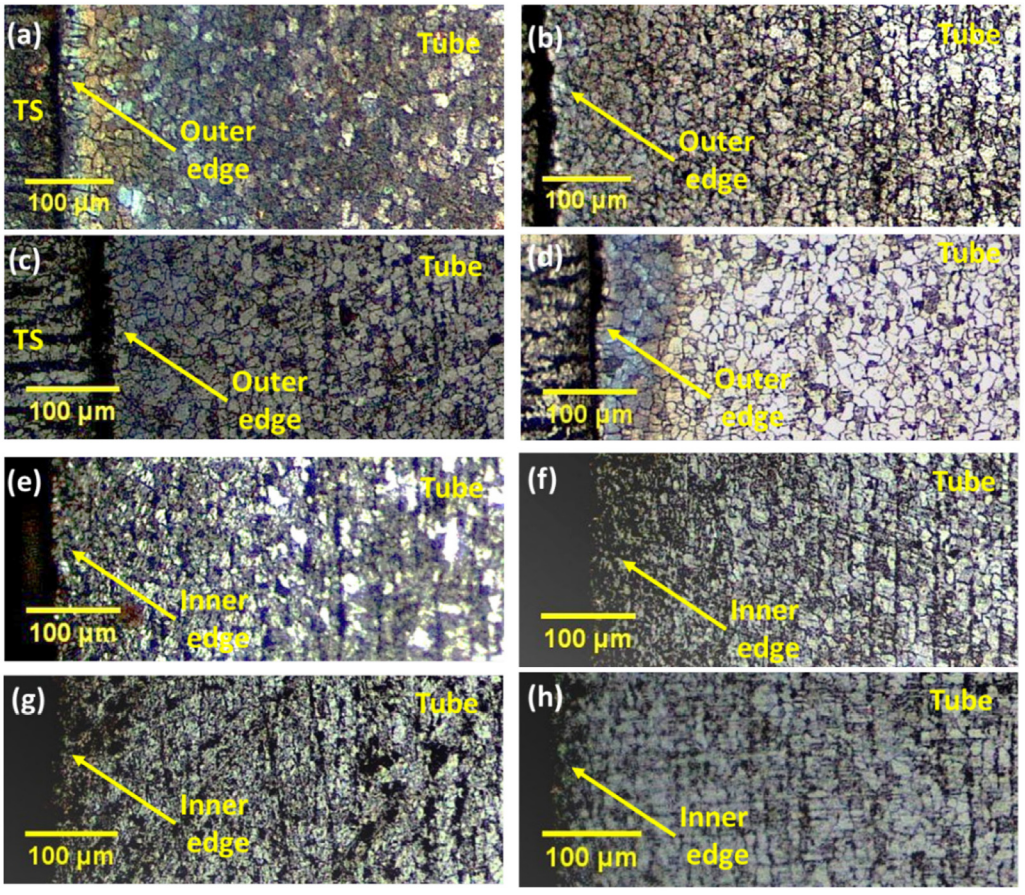

Fig. 14 – Microstructures at the outer tube edge of the expanded zone: (a) 4% expansion percentage, (b) 6% expansion percentage, (c) 8% expansion percentage and (d) 10% expansion percentage. Microstructures at the inner tube edge of the expanded zone: (e) 4% expansion percentage, (f) 6% expansion percentage, (g) 8% expansion percentage and (h) 10% expansion percentage.

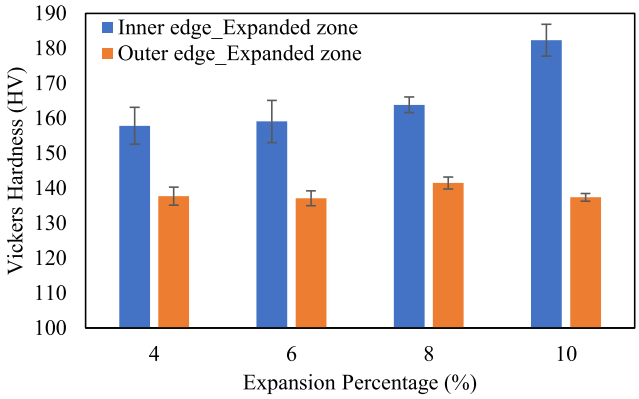

Fig. 15 – Hardness at the inner and outer tube edges of expanded zone.

outer tube surface has resulted in exhibiting a smaller grain size of 7.69 μm. Fig. 15 shows the hardness with standard error at the inner tube edge and outer edge of the expanded zone. The hardness at the outer tube edge at 4%, 6%, 8% and 10% expansion percentages were 137.7 HV, 137.1 HV, 141.4 HV and 137.3 HV respectively. The hardness at the outer tube edge at four expansion percentages was nearly the same. The tube is subjected to compression during the wall thinning of the tubes. The compressive force is exerted on the inner tube surface by the rollers whereas the compression of the tube against the tubesheet imparts compressive stress on the outer tube surface. However, it is found that the grains at the outer tube surface are not intensively refined. This may be due to the pressure exerted at the tube-to-tubesheet interface being uniform once all the outer tube surface comes in contact with the tubesheet. At the same time, the inner tube surface was expanded using rollers in the form of cyclic loads. The rolling action was proved to increase the hardness by the degree of cold work and strain hardening [52]. The compressive residual stress during work hardening is known for the increase in the hardness [53]. However, the exhibition of low hardness at the outer tube edge and high hardness at the inner tube edge is concluded to be mainly due to the type of loading conditions.

The inner tube surface was rolled radially outwards using rollers in the roller expansion process. The grain size at the inner tube edge for the cases of 4%, 6%, 8% and 10% expanded conditions was 8.33 μm, 7.14 μm, 6.66 μm and 6.25 μm respectively. It is noticed that the grain size was reduced with

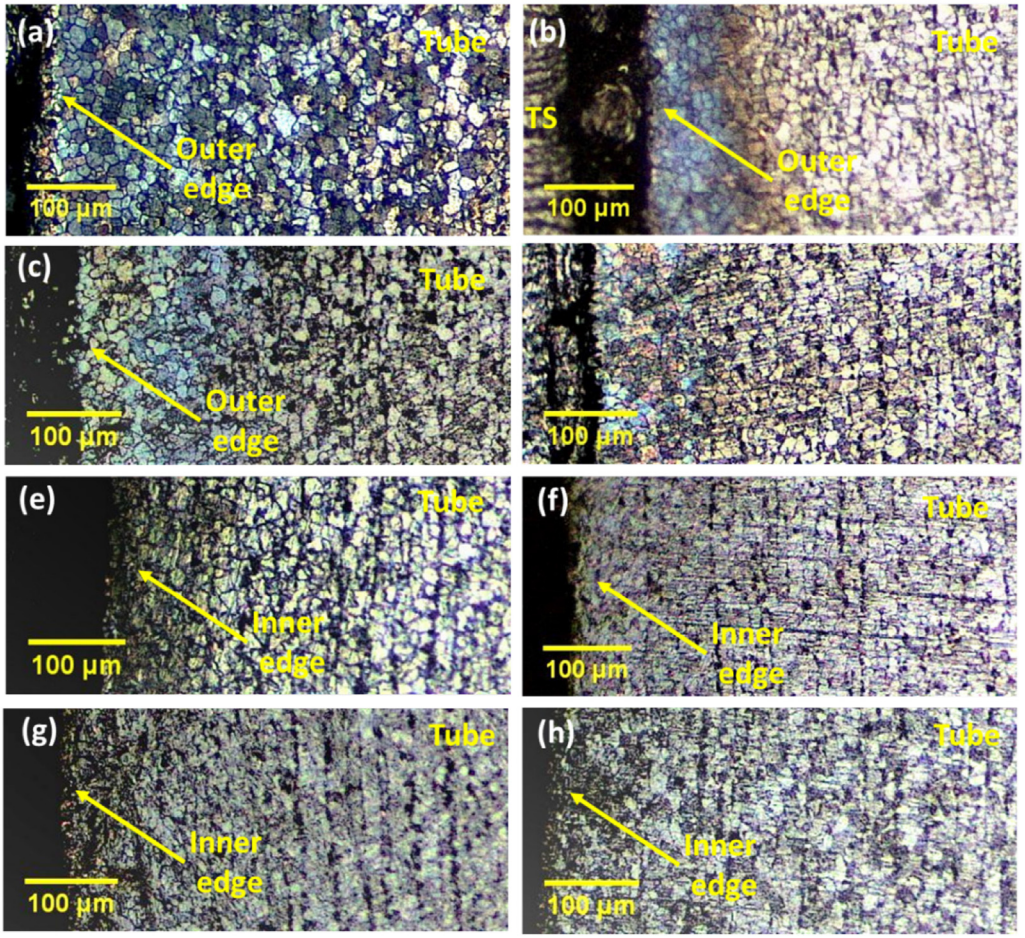

Fig. 16 – Microstructures at the outer tube edge of the transition zone: (a) 4% expansion percentage, (b) 6% expansion percentage, (c) 8% expansion percentage and (d) 10% expansion percentage. Microstructures at the inner tube edge of the transition zone: (e) 4% expansion percentage, (f) 6% expansion percentage, (g) 8% expansion percentage and (h) 10% expansion percentage.

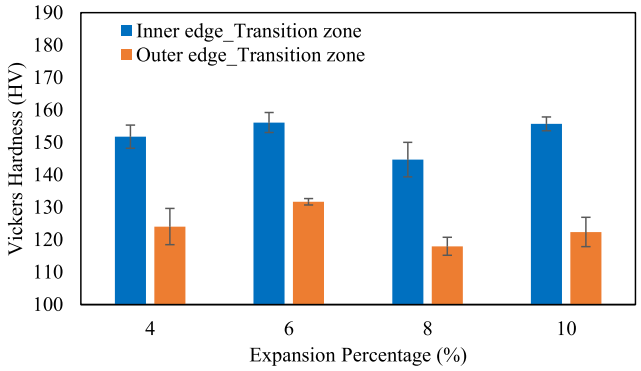

Fig. 17 – Hardness at the inner and outer edges of the transition zone.

the increase in the roller expansion percentage. There is a clear reduction in the grain sizes at higher expansion pressures. On the other hand, the hardness was also increased with the reduction in the grain size and increase in the expansion percentage at the inner tube edges. In this case, the relationship between the hardness and grain size proved that the grain size is inversely proportional to hardness [54]. The hardness at the inner tube edge increased only slightly from 157.8 HV to 163.8 HV for the expansion percentage from 4% to 8% whereas the hardness abruptly increased up to 182.3 HV at a 10% expansion percentage. The high hardness at 10% expansion is due to high grain dislocation density and grain refinement as a result of the severe wall thinning phenomenon [55]. The comparison of the grain sizes at the inner and outer tube edges indicated that the grain size reduction is predominant at the inner tube edge rather than at the outer tube edge. The influence of the roller expansion effect is greater than the contact stress at the tube-to-tubesheet interface.

Figs. 16 and 17 show microstructure at the transition zone and, mean hardness with standard error at the transition zone. In the transition zone and outer tube edges, the grain sizes for 4% and 6% expanded conditions are 10 μm. However, there is an abrupt reduction of grain size at 10% expanded condition to 6.66 μm. The hardness at 4%, 6%, 8% and 10% expansion percentages were 124 HV, 131.7 HV, 117.9 HV and 122.3 HV respectively. It is to be noted that the hardness for all conditions was within 132 HV. The reduction of hardness at the transition zone at the outer tube edge compared to the expanded zone is due to the absence of tube contact with the tubesheet and thereby lacking the compressive stress at the outer edge. In the transition zone and inner tube edges, the grain size is lesser at the inner tube edges compared to outer tube edges at lower expansion percentages of 4% and 6%. The grain sizes at 4% and 6% are 9.09 μm and 8.33 μm, respectively. But at higher expansion percentages of 8% and 10%, grain sizes of 8.33 μm and 6.66 μm at the inner tube edge of the transition zone were slightly higher than at the outer tube edges of the transition zone. The hardness at the inner tube edge of the transition zone was 151.7 HV, 156.1 HV, 144.7 HV and 155.7 HV for 4%, 6%, 8% and 10% expansion percentage conditions. The hardness at the inner tube edge of the transition zone is high compared to the hardness of base materials, but the hardness at this transition zone is slightly lesser than at the expanded zone in the inner tube edges. It is noted that there is a significant difference in the hardness between the inner tube edge and the outer tube edge at the transition zone.

4. Conclusion

The research investigated the mutual effect of expansion percentages (4%, 6%, 8% and 10%) and groove conditions (without groove, one groove and two grooves) on the mechanical and metallurgical properties of mainly the expanded and hybrid welded-expanded tube-to-tubesheet joints. The welded tube-to-tubesheet joints are produced to compare the tube pull-out load with the expanded and hybrid welded-expanded tube-to-tubesheet joints. The major findings are provided as following bullet points.

- The failure of hybrid welded-expanded joint with 6% expansion percentages and two grooves' conditions indicated that poor weld workmanship, high dilution, lack of weld penetration or lack of minimum leak path reduce the joint strength significantly.
- In the absence of welding and for the expanded only joints, the tubes slipped out from the tubesheet during the tube pull-out test for all conditions with expansion percentage ranging from 4% to 10% and all groove conditions. The expanded joints were disqualified as a result of the joint strength lesser than the axial tube strength.
- The expansion length of 23 mm over the entire tubesheet thickness was insufficient for achieving quality expanded only joints. Therefore, tubesheet thickness and expansion length were found as important factors significantly affecting the strength of expanded shell and tube heat exchanger tube-to-tubesheet joints. It is recommended to use thick tubesheet greater than 23 mm for the heat exchangers that are explicitly manufactured using expansion process alone.
- The welded tube-to-tubesheet joints exhibited joint strength greater than the axial tube strength. The tube fracture rather than joint fracture indicated the presence of sufficient joint strength. Welding as a stand-alone operation for shell and tube heat exchanger tube-to-tubesheet joints is the optimum manufacturing process compared to hybrid welded-expanded and expanded processes.
- The welds, except for the condition of 8% tube expansion and 1 groove, in hybrid welded and expanded joints were qualified with minimum leak path greater than two-thirds of tubesheet thickness (1.78 mm) as per ASME SEC IX - Clause QW-193.1.3. High dilution and lack of sufficient minimum leak path for welded-expanded 6%-2G condition is anticipated for the weld joint rupture in the tube pull-out test.
- The microstructure of ASTM A179 tubes constituted pearlite colonies in ferrite microstructure whereas the microstructure of SA 517 Gr. 70 comprised of equiaxed ferrite and banded pearlite. The weld zone was comprised of polygonal ferrite, pearlite and widmanstätten ferrite

(WF). The α-ferrite (ICDD 98-006-0826) was present in the weld zone whereas the δ-ferrite and γ-ferrite were not formed at the weld zone.

- The presence of widmanstätten ferrite and alloying elements from the electrode at the weld zone contributed for the exhibition of high weld hardness of 218 HV.
- In the expanded and transition zone, the intensity of grain refinement was severe at the inner tube edges by the action of rollers than at the outer tube edges that eventually comes in contact with the tubesheet during expansion process.
- The coarser grain sizes of 10 μm and 9.09 μm at the outer edge of the expanded tube zone at 4% and 6% expansion percentages are considered as an indication of insufficient contact pressure between tube and tubesheet in the expansion process.
- The hardness of the tube at the expanded zone at the inner tube edges increased with the expansion percentage while the hardness was nearly constant at the outer tube edges.
- The reduction of hardness at the transition zone at the outer tube edge compared to the expanded zone is due to the absence of tube contact with the tubesheet and thereby lacking the compressive stress at the outer edge.
- The hardness at the inner tube edge of transition zone is high compared to the hardness of base materials, but the hardness at this transition zone is slightly lesser than at the expanded zone in the inner tube edges.

The future scopes of the work are to conduct experimental investigations for evaluating the influence of tubesheet thickness, expansion roller length, the comparison between the roller expansion process and hydraulic expansion process, the impact of hybrid welding-hydraulic expansion process on tube-to-tubesheet characteristics and estimating the performance of high pressure-high temperature operating shell and tube heat exchanger tube-to-tubesheet joints using inconel alloys and titanium alloys.

Declaration of competing interest

The authors declare that they have no known competing financial interests or personal relationships that could have appeared to influence the work reported in this paper.

Acknowledgement

The project was supported and funded by United Arab Emirates University [Grant # 31R105].

REFERENCES

[1] Chengjun J, Xin W, Xiaolong X. Welding procedure research of zirconium tube-to-tubesheet. In: J. Phys. Conf. Ser. IOP Publishing; 2021, 12043.
[2] Mourad AHI, Khourshid A, Sharef T. Gas tungsten arc and laser beam welding processes effects on duplex stainless steel 2205 properties. Mater Sci Eng A 2012;549:105–13. https://doi.org/10.1016/j.msea.2012.04.012.
[3] Farrahi GH, Minaii K, Chamani M, Mahmoudi AH. Effect of residual stress on failure of tube-to-tubesheet weld in heat exchangers. Int J Eng 2019;32:112–20.
[4] Corleto CR, Argade GR. Failure analysis of dissimilar weld in heat exchanger. Case Stud Eng Fail Anal 2017;9:27–34.
[5] Talabi SIA, Owolabi OBB, Adebisi JAA, Yahaya TA. Effect of welding variables on mechanical properties of low carbon steel welded joint. Adv Prod Eng Manag 2014;9:181–6.
[6] Saffiudeen MF, Syed A, Mohammed FT. Failure analysis of heat exchanger using internal rotary inspection system (IRIS). J Fail Anal Prev 2021;21:494–8.
[7] Bouzid A-H, Kazeminia M. Effect of reverse yielding on the residual contact pressure in tube-to-tubesheet joints. J Pressure Vessel Technol 2016;138.
[8] Elliott tool technologies, Tube expander design & usage, (n.d.). https://www.elliott-tool.com/tube-expander-design-usage/(accessed July 16, 2022).
[9] Yoganathan R, Ramanathan A. An experimental study of effects on tube to tube sheet expansion joint grip strength due to seal welding or blanking of adjacent bank tubes of bi-drum boiler. Mater Today Proc 2021;46:9328–33.
[10] Saffiudeen MF, Mohammed FT, Syed A. A case study on procedure standardization of heat exchanger retubing in KSA oil and gas industries. J Fail Anal Prev 2020;20:1451–5.
[11] Thekkuden DT, Mourad A-HI, Bouzid A-H. Impact of grooves in hydraulically expanded tube-to-tubesheet joints. In: ASME 2020 press. Vessel. Pip. Conf. American Society of Mechanical Engineers Digital Collection; 2020.
[12] Ma H, Yu HJ, Qian CF, Liu ZS, Zhou JX. Experimental study of hydraulically expanded tube-to-tubesheet joints for shell-and-tube heat exchangers. Procedia Eng 2015;130:263–74. https://doi.org/10.1016/j.proeng.2015.12.220.
[13] Wang HF, Sang ZF. Effect of geometry of grooves on connection strength of hydraulically expanded tube-to-tubesheet joints. J Pressure Vessel Technol 2005;127:430. https://doi.org/10.1115/PVP2004-2600.
[14] Qian C, Duan C, Yu H, Duan H, Tian J. Reliability study of the hydraulically expanded tube-to-tubesheet joint. 2006.
[15] Yoganathan R, Shanmugam NS, Ramanathan A. Effects of thickness offset on the tube-to-tube sheet expansion joint strength: an experimental evaluation. J Mater Eng Perform 2021:1–13.
[16] Wei XL, Ling X. Investigation of welded structures on mechanical properties of 304L welded tube-to-tubesheet joints. Eng Fail Anal 2015;52:90–6.
[17] Al-Aboodi A, Merah N, Shuaib AN, Al-Nassar Y. Effects of friction on roller expanded tube-tubesheet joint strength. Int J Material Form 2010;3:253–7. https://doi.org/10.1007/s12289-010-0686-3.
[18] ThomasThekkuden D, Mourad A-HI, Bouzid A-H, Darabseh T. Impact of expansion pressure on wall thinning and contact pressure for hydraulically expanded tube-to-tubesheet joints: numerical analysis. In: 2020 adv. Sci. Eng. Technol. Int. Conf. IEEE; 2020. p. 1–6.
[19] Bouzid AH, Mourad AHI, El Domiaty A. Influence of Bauschinger effect on the residual contact pressure of hydraulically expanded tube-to-tubesheet joints. Int J Press Vessel Pip 2016;146:1–10. https://doi.org/10.1016/j.ijpvp.2016.07.002.
[20] Bouzid A-H, Zhu L. A study of neighbouring tube expansion effect on the residual contact pressure of tube-to-tubesheet joints. Int J Press Vessel Pip 2018;165:185–92.
[21] Alaboodi AS. Finite element study of the hybrid expansion of tube-to-tubesheet joints. Thin-Walled Struct 2019;137:347–52.

[22] Bouzid A-H, Pourreza M. Analysis of residual stresses in the transition zone of tube-to-tubesheet joints. J Pressure Vessel Technol 2019;141.
[23] Kiptisia W, Namgung I. Analysis of residual stresses on the expanding transition zone of steam generator tubes of Apr1400. J Press Vessel Technol 2019.
[24] Mohammadi Zahrani E. Premature failure of grade-316Ti stainless steel tubing in a boiler feed-water heat exchanger in a steel complex. J Fail Anal Prev 2021;21:61–73.
[25] Sui R, Zhao Y, Ge B, Wang W. Failure analysis of leakage at tube-to-tubesheet joints of a waste heat boiler. Eng Fail Anal 2021;129:105639.
[26] Thekkuden DT, Mourad A-HI, Bouzid A-H. Failures and leak inspection techniques of tube-to-tubesheet joints: a review. Eng Fail Anal 2021;130:105798.
[27] Yokell S. Assuring tube-to-tubesheet joint tightness and strength. J Press Vessel Technol 2012;134.
[28] Adullah S, Ezuber HM. Repair of tube–tubesheet weld cracks in a cracked gas/steam heat exchanger. J Fail Anal Prev 2011;11:611–7.
[29] ASME. 2010 ASME boiler & pressure vessel code: VIII,division 1, rules for construction of pressure vessels. Asme; 2010. p. 1–746.
[30] Boiler A, Code PV. Section VIII: rules for construction of pressure vessels, division 1. New York: Am. Soc. Mech. Eng. (ASME); 2019. p. 585–91.
[31] García González J, Hernández-Ortega JJ, Jiménez-Ballesta A-E, Pedreño RZ. Analysis of tube-to-tubesheet welding in carbon steel heat exchangers of a double plate header box. Materials 2021;15:261.
[32] Thekkuden DT, Santhakumari A, Sumesh A, Mourad A-HI, Rameshkumar K. Instant detection of porosity in gas metal arc welding by using probability density distribution and control chart. Int J Adv Manuf Technol 2018;95:4583–606.
[33] González-Gómez PA, Gómez-Hernández J, Ruiz C, Santana D. Can solar tower plants withstand the operational flexibility of combined cycle plants? Appl Energy 2022;314:118951.
[34] Pouraliakbar H, Khalaj G, Jandaghi MR, Khalaj MJ. Study on the correlation of toughness with chemical composition and tensile test results in microalloyed API pipeline steels. J Min Metall B Metall 2015;51:173–8.
[35] Khalaj G, Azimzadegan T, Khoeini M, Etaat M. Artificial neural networks application to predict the ultimate tensile strength of X70 pipeline steels. Neural Comput Appl 2013;23:2301–8.
[36] Merah N, Al-Aboodi A, Shuaib AN, Al-Nassar Y. 3-D finite element analysis of roller-expanded heat exchanger tubes in over-enlarged tubesheet holes. Appl Petrochem Res 2012;1:45–52. https://doi.org/10.1007/s13203-011-0005-z.
[37] Sang ZF, Zhu YZ, Method E. Reliability factors and tightness of tube-to-tubesheet joints. J Pressure Vessel Technol 1996;118:137–41.
[38] Boiler A, Code PV. Section IX: welding and brazing qualifications, paragraph QW-290, temper bead welding. ASME; 2004.
[39] Saffiudeen MF, Mohammed FT, Syed A. Comparative study of tube to tubesheet welding qualification on heat exchanger. J Eng Appl Sci 2022;69:1–14.
[40] Herold H, Zinke M, Huebner A, Schilling K, Boese E, Goellner J. Relations between dilution and characteristics of over-alloyed welded seams on super duplex stainless steel. Weld World 2007;51:3–14.
[41] Kumar V, Lee C, Verhaeghe G, Raghunathan S. CRA Weld Overlay-Influence of welding process and parameters on dilution and corrosion resistance. USA: Houst. Stainl. Steel World Am. Texas; 2010. p. 64–71.
[42] Muhayat N, Matien YA, Sukanto H, Saputro YCN. Fatigue life of underwater wet welded low carbon steel SS400. Heliyon 2020;6:e03366.
[43] Mohsenzadeh MS, Mazinani M. On the yield point phenomenon in low-carbon steels with ferrite-cementite microstructure. Mater Sci Eng A 2016;673:193–203.
[44] Zhao Y, Wang Q, Chen H, Yan K. Microstructure and mechanical properties of spray formed 7055 aluminum alloy by underwater friction stir welding. Mater Des 2014;56:725–30.
[45] Khalaj G, Yoozbashizadeh H, Khodabandeh A, Tamizifar M. Austenite grain growth modelling in weld heat affected zone of Nb/Ti microalloyed linepipe steel. Mater Sci Technol 2014;30:424–33.
[46] Khalaj G, Nazari A, Pouraliakbar H. Prediction of martensite fraction of microalloyed steel by artificial neural networks. Neural Netw World 2013;23:117.
[47] Bhadeshia H, Svensson LE. Modelling the evolution of microstructure in steel weld metal. Math Model Weld Phenom 1993;1:109–82.
[48] Milliams DE, Cottage D, Tuttle RN. ISO 15156/NACE MR0175-A new international Standard for metallic materials for use in oil and gas production in sour environments. In: Corrosion 2003. OnePetro; 2003.
[49] Beer D, Johan D. The relationship of weld metal hardness residual stress and susceptible to stress corrosion cracking in hydrogen sulphide environment in A516 Grade 70 carbon steel shielded metal arc welded joint. 2019.
[50] Bose-Filho WW, Carvalho ALM, Strangwood M. Effects of alloying elements on the microstructure and inclusion formation in HSLA multipass welds. Mater Charact 2007;58:29–39.
[51] Cho Y, Lee J, Kim D, Kang J, Choo WY, Han HN. Ferrite phase analysis based on low-angle grain boundary density in low carbon linepipe steel. In: Proc. 5th Int. Symp. Steel Sci. (ISSS 2017); 2017. p. 203–6.
[52] Shuaib AN, Merah N, Khraisheh MK, Allam IM, Al-Anizi SS. Experimental investigation of heat exchanger tubesheet hole enlargement. J Pressure Vessel Technol 2003;125:19–25.
[53] GoKYU I, KisHI T. Warm working of metals and alloys. Bull JSME 1969;12:630–7.
[54] Jung B, Lee H, Park H. Effect of grain size on the indentation hardness for polycrystalline materials by the modified strain gradient theory. Int J Solid Struct 2013;50:2719–24.
[55] Ağca S, Çankaya G. The effect of cold rolling on mechanical properties of zircaloy-4. Int J Multidiscip Stud Innov Technol 2017;1:29–35.